Journal of Power Sources 202 (2012) 63–69

Contents lists available at SciVerse ScienceDirect

Journal of Power Sources

journal homepage: www.elsevier.com/locate/jpowsour

Synthesis and characterization of Mo-doped $SrFeO_{3-\delta}$ as cathode materials for solid oxide fuel cells

Guoliang Xiao[a], Qiang Liu[a], Siwei Wang[a], Vasileios G. Komvokis[b], Michael D. Amiridis[b], Andreas Heyden[b], Shuguo Ma[c], Fanglin Chen[a,*]

[a] Department of Mechanical Engineering, University of South Carolina, Columbia, SC 29208, United States
[b] Department of Chemical Engineering, University of South Carolina, Columbia, SC 29208, United States
[c] College of Engineering and Computing, University of South Carolina, Columbia, SC 29208, United States

ARTICLE INFO

Article history:
Received 27 September 2011
Received in revised form 5 November 2011
Accepted 7 November 2011
Available online 15 November 2011

Keywords:
Strontium ferrite
Perovskite
Conductivity
Cathode
Solid oxide fuel cells

ABSTRACT

This paper demonstrates the potential application of Mo-doped $SrFeO_{3-\delta}$ perovskites as new cathode materials for solid oxide fuel cells (SOFCs). $SrFe_{1-x}Mo_xO_{3-\delta}$ ($x = 0$, 0.05, 0.1, 0.2 and 0.25) perovskite materials have been synthesized by a microwave-assisted combustion method. By doping with Mo, the electrical conductivity of the doped $SrFeO_{3-\delta}$ in air is reduced with increasing amounts of Mo. At 800 °C, the conductivity drops from about 62 to 22 S cm^{-1} when the doping level is increased to 25%. According to X-ray diffraction (XRD), X-ray photoelectron spectroscopy (XPS) and temperature programmed reduction (TPR) results, a decrease in the concentration of charge carrier Fe^{4+} ions may account for the decrease in electrical conductivity. In contrast, the resistance to sintering and tolerance to reduction of $SrFeO_{3-\delta}$ are improved by Mo-doping. Additionally, the thermal expansion coefficient at 800 °C drops from 40.8×10^{-6} K^{-1} for $SrFeO_{3-\delta}$ to 25.7×10^{-6} K^{-1} for $SrFe_{0.8}Mo_{0.2}O_{3-\delta}$ and 20.9×10^{-6} K^{-1} for $SrFe_{0.75}Mo_{0.25}O_{3-\delta}$. This significant decrease in the thermal expansion coefficient makes Mo-doped $SrFeO_{3-\delta}$ materials attractive as cathode candidates for SOFCs. Finally, a relatively low polarization resistance of 0.074 Ω cm^2 is obtained for $SrFe_{0.8}Mo_{0.2}O_{3-\delta}$ at 800 °C in air.

1. Introduction

The development of energy related techniques becomes more and more important as the world's demand for energy is increasing. Solid oxide fuel cell (SOFC) technology has been considered as one of the most promising energy generation techniques which can directly convert the chemical energy of the fuel into electricity with high efficiency and low emissions [1]. Currently, the development of SOFCs requires advanced cathode, anode and electrolyte materials, especially at reduced operating temperatures [2].

Perovskite $SrFeO_{3-\delta}$ is an interesting material which exhibits high mixed oxide ionic and electronic conductivity and therefore can be potentially used in electrochemical devices such as oxygen permeation membranes, oxygen sensors, and SOFCs [3–5]. It is also an instructive model whose crystal structure and electronic properties are sensitively related to the oxygen vacancy ordering. Fe cations in this system are in a mixed valence state ranging from +4 to +3, corresponding to a wide range of oxygen non-stoichiometry (from 0 to 0.5), while the structure changes from cubic to orthorhombic brownmillerite type with long range ordering oxygen vacancies [6–8]. Recently, an infinite-layer compound $SrFeO_2$ has also been reported [9]. However, the tendency of formation of ordered oxygen vacancies is not favorable for practical applications because it hinders oxygen transfer, while the oxygen deficiency also results in a decrease in both mobility and concentration of hole carriers [10,11]. Therefore, modifications of the $SrFeO_{3-\delta}$ system are necessary for different applications.

Many important electrode materials for SOFCs can be derived from $SrFeO_{3-\delta}$ by doping with other cations [5,12–14]. Recently, Mo-doped $SrFeO_{3-\delta}$ has become a subject of intensive studies. Molybdenum ions show higher valence than iron ions so that Mo-doping can strongly affect the iron oxidation states and the simultaneous formation of oxygen defects in the provskite which are responsible for the catalytic activity and the electrical properties. Therefore, Mo-doped $SrFeO_{3-\delta}$ shows quite different properties for different Mo-doping contents. At high Mo-doping levels, double perovskite $SrFe_{1-x}Mo_xO_{3-\delta}$ ($0.25 < x < 0.6$) with ordered Fe and Mo in the B site has been obtained in reducing atmospheres and showed good performance as an anode material in SOFCs [15–17]. At lower Mo-doping levels, $SrFe_{1-x}Mo_xO_{3-\delta}$ ($0.05 \le x \le 0.25$) is in a simple cubic perovskite structure in air and can be potentially applied for oxygen permeation [18,19]. More interestingly, in this low Mo-doping range, Mo-doped $SrFeO_{3-\delta}$ also

* Corresponding author. Tel.: +1 803 777 4875; fax: +1 803 777 0106.
E-mail address: chenfa@cec.sc.edu (F. Chen).

0378-7753/$ – see front matter © 2011 Elsevier B.V. All rights reserved.
doi:10.1016/j.jpowsour.2011.11.021

shows good stability in a wide range of oxygen partial pressures and $SrFe_{0.75}Mo_{0.25}O_{3-\delta}$ has been demonstrated as a redox stable electrode for SOFCs [20,21]. These results promote interests in studying Mo-doped $SrFeO_{3-\delta}$ perovskites as new cathode materials.

In this work, the doping effects of Mo on properties of $SrFe_{1-x}Mo_xO_{3-\delta}$ materials in the low doping range ($0 \le x \le 0.25$) have been systematically studied. The samples have been prepared by a combustion method [20]. The Mo-doping effects on the electrical properties have been investigated through measurements of the electrical conductivities as well as X-ray photoelectron spectroscopy (XPS) analyses. Furthermore, the reduction behavior has been evaluated by temperature programmed reduction (TPR) measurements. Finally, the thermal expansion behavior and polarization resistance have also been studied, since these are important properties for potential cathode materials for SOFCs.

2. Experimental

$SrFe_{1-x}Mo_xO_{3-\delta}$ ($x = 0$, 0.05, 0.1, 0.2 and 0.25) powders were synthesized by a microwave-assisted combustion method. $Sr(NO_3)_2$, $Fe(NO_3)_3{\cdot}9H_2O$ and $(NH_4)_6Mo_7O_{24}{\cdot}4H_2O$ were used as metal precursors. Glycine and citric acid were used as fuels. Single-phased powders were obtained by firing the as-prepared ash at 1000 °C for 5 h. $La_{0.8}Sr_{0.2}Ga_{0.87}Mg_{0.13}O_3$ (LSGM) powder used in this experiment was synthesized by solid-state reaction.

Electrical conductivity measurements were performed using a dc four-probe method on sintered rectangular dense bars. In a typical process, 2 g of the powder was put into a die with 45 mm length and 6 mm width and uniaxially pressed into a green bar. The green bar was buried in the powder to prevent Mo-evaporation and then sintered at 1300 °C in air for 6 h. Thermal expansion coefficients were also measured on the rectangular bars prepared in the same way. According to the standard alumina sample size, the bars were cut into a smaller piece of 12 mm in length before the thermal expansion coefficient measurement.

The LSGM powder was pressed into pellets as the electrolyte for symmetrical half cells. The pellets were sintered at 1450 °C for 10 h in air to obtain dense LSGM pellets. Electrode powders were mixed with a Heraeus binder V006 (weight ratio of 1:1.5) as electrode inks which were painted on each side of the LSGM pellets to form symmetric half cells. The electrodes were all fired at 1100 °C in air for 2 h. Before testing, Pt paste was applied onto the electrodes as the current collector and fired at 1000 °C in air for another 0.5 h.

Phase purity and structure of the prepared materials were investigated by a D/MAX-3C X-ray diffractometer with graphite-monochromatized CuKα radiation (λ = 1.5418 Å) scanning from 20° to 80° at a rate of 5° min^{-1}. Microstructure and morphology of the samples were characterized by scanning electron microscopy (SEM, FEI Quanta 200). XPS measurements were conducted on the powders using a Kratos Axis Ultra DLD instrument. The XPS spectra were calibrated by the C1 s signal at 284.6 eV. TPR was performed on powders. The samples were degased at 400 °C in N_2 and oxidized in a 10% O_2/N_2 mixture before testing. The TPR profiles were recorded in a 5% H_2/Ar mixture with a ramp rate of 10 °C min^{-1}. Thermogravimetry (TG) was performed with a NETZSCH model STA 409 instrument from room temperature to 1000 °C with a heating rate of 10 °C min^{-1} in a flowing 5% H_2/Ar mixture following the same protocol with the TPR experiments. Thermal expansion coefficients (TECs) were measured with a dilatometer (Netsch DLL 402C/3/G) from room temperature to 1000 °C, with an air-purge flow rate of 50 ml min^{-1}. Impedance spectra of symmetrical cells were measured with an electrochemistry workstation (IM6-Zahner) at different temperatures in air with a flow rate of 60 ml min^{-1}.

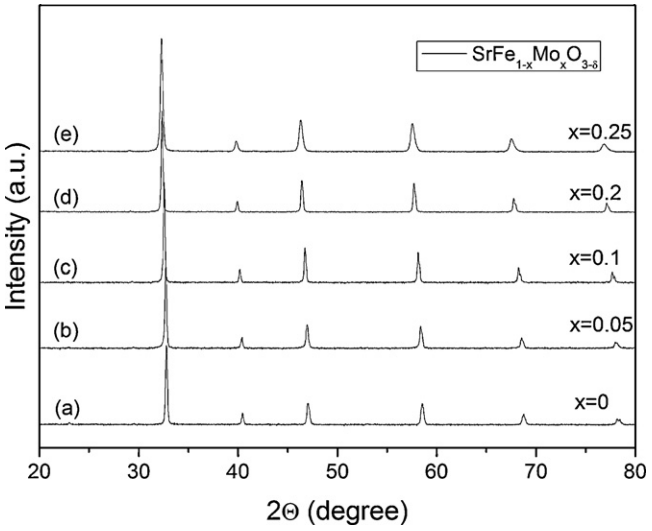

Fig. 1. XRD patterns of $SrFe_{1-x}Mo_xO_{3-\delta}$ powders: (a) $x = 0$, (b) $x = 0.05$, (c) $x = 0.1$, (d) $x = 0.2$, and (e) $x = 0.25$.

3. Results and discussion

Phase and structure of $SrFe_{1-x}Mo_xO_{3-\delta}$ ($x = 0$, 0.05, 0.1, 0.2 and 0.25) powders were studied by XRD. As shown in Fig. 1, all samples exhibit well-defined reflections and no impurity peak can be observed. With increasing Mo doping ratio, all peaks shift to lower diffraction angles indicating that the Mo content has a big influence on the crystal structure. For $SrFeO_{3-\delta}$, the crystal structure was reported to be strongly related to the concentration and arrangement of oxygen vacancies, which depend on temperature and oxygen partial pressure. The known phases can be described as $Sr_nFe_nO_{3n-1}$ ($n = \infty$, 8, 4, 2, 1) corresponding to cubic, tetragonal, orthorhombic, brownmillerite-type and infinite-layer type structures [6,9]. However, due to the weak scattering of X-rays on oxygen atoms, no clear difference can be observed in the XRD patterns of $SrFeO_{3-\delta}$ with different oxygen content [22]. The structure of Mo-doped $SrFeO_{3-\delta}$ can be indexed into cubic perovskite even at the lowest doping level of $x = 0.05$ [18]. Therefore, the cell parameters of $SrFe_{1-x}Mo_xO_{3-\delta}$ ($x = 0$, 0.05, 0.1, 0.2 and 0.25) were all calculated in the cubic structure (*Pm*-3*m*). As shown in Fig. 2, the lattice parameters, which increase gradually with increasing Mo content, appear to follow Vagard's law. However, Mo^{6+} (0.59 Å)

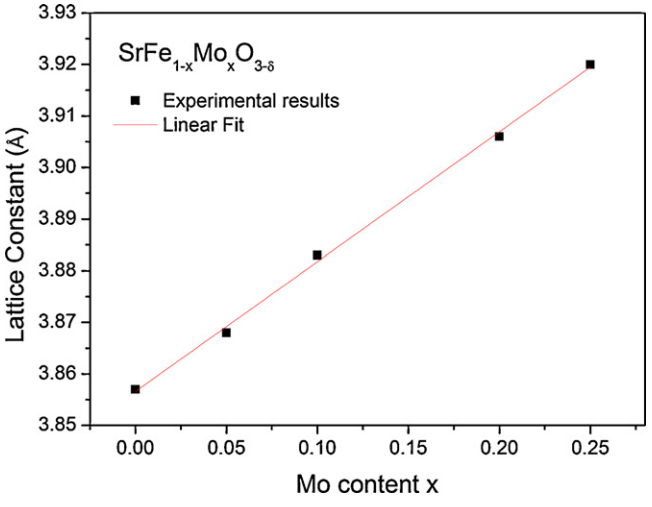

Fig. 2. Dependence of lattice parameters on Mo doping.

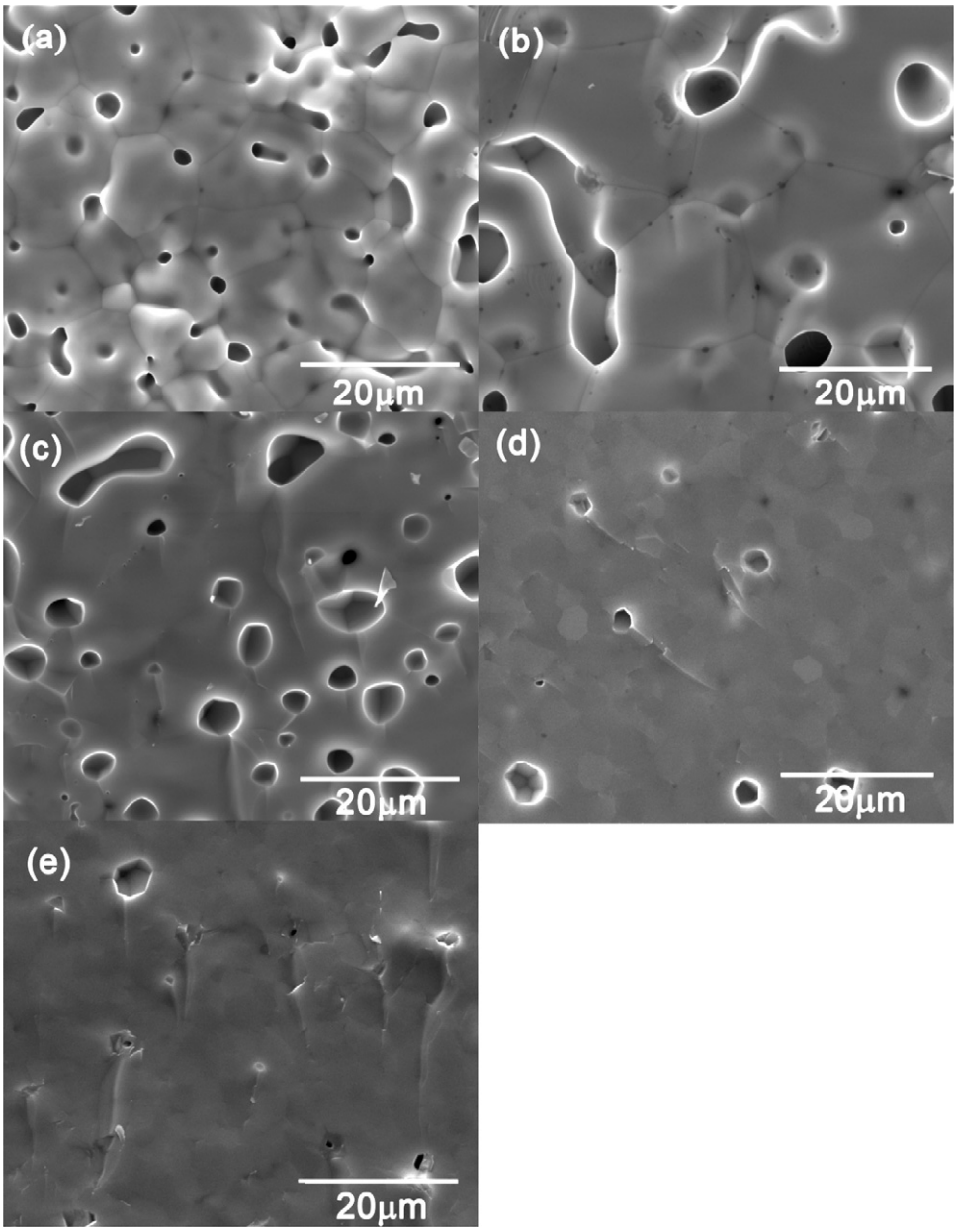

Fig. 3. SEM images captured on the fracture surfaces of $SrFe_{1-x}Mo_xO_{3-\delta}$ bars: (a) $x = 0$, (b) $x = 0.05$, (c) $x = 0.1$, (d) $x = 0.2$, and (e) $x = 0.25$.

has a very similar ionic radius to Fe^{4+} (0.585 Å). Therefore, the lattice expansion is probably due to the reduction of Fe^{4+} cations to Fe^{3+} cations. Such reduction may be considered as the charge compensation for the incorporation of Mo^{6+} in the crystal lattice. Additionally, it is also noticeable that the crystallinities are different for different samples examined. As seen from Fig. 1, the peak intensity increases with Mo-doping under the same synthesis conditions indicating higher crystallinity in the samples with higher Mo content.

Different shrinkage of the $SrFe_{1-x}Mo_xO_{3-\delta}$ ($x = 0$, 0.05, 0.1, 0.2 and 0.25) bars after sintering was observed suggesting that the sintering behavior of $SrFeO_{3-\delta}$ is also changed by Mo-doping. The fracture surface of the bars was investigated by SEM after testing and characteristic images are shown in Fig. 3. Apart from the pits created by fraction, more interconnected holes can be observed on the $SrFeO_{3-\delta}$ bar. The relative densities of the bars were also found to increase from 88% for the $SrFeO_{3-\delta}$ bar to approximately 95% for the $SrFe_{0.75}Mo_{0.25}O_{3-\delta}$ bar under same preparation conditions. These results suggest that Mo-doping may increase the sinterability of $SrFeO_{3-\delta}$.

Element distribution of the $SrFe_{0.8}Mo_{0.2}O_{3-\delta}$ bar was studied by EDX equipped on SEM. Fig. 4a shows well-defined crystal grains and boundaries and Fig. 4b–d shows element mapping results obtained on the fracture surface. The distribution of Sr, Fe and Mo are homogeneous and no phase segregation is observed.

Fig. 5 shows the electrical conductivities of $SrFe_{1-x}Mo_xO_{3-\delta}$ ($x = 0$, 0.05, 0.1, 0.2 and 0.25) samples measured in air from 400 °C to 850 °C using a four-probe method. As shown in Fig. 5a, $SrFeO_{3-\delta}$ exhibits the highest conductivity in the whole temperature range and the value drops with increase in Mo-doping. According to the literature, $SrFeO_{3-\delta}$ shows a p-type conducting behavior when the oxygen partial pressure is above 10^{-5} atm [18]. The relationship between the charge carrier Fe^{4+} and oxygen vacancies can be expressed as:

$$2Fe_{Fe}^{\times} + V_O^{\bullet\bullet} + \frac{1}{2}O_2 \leftrightarrow 2Fe_{Fe}^{\bullet} + O_O^{\times} \quad (1)$$

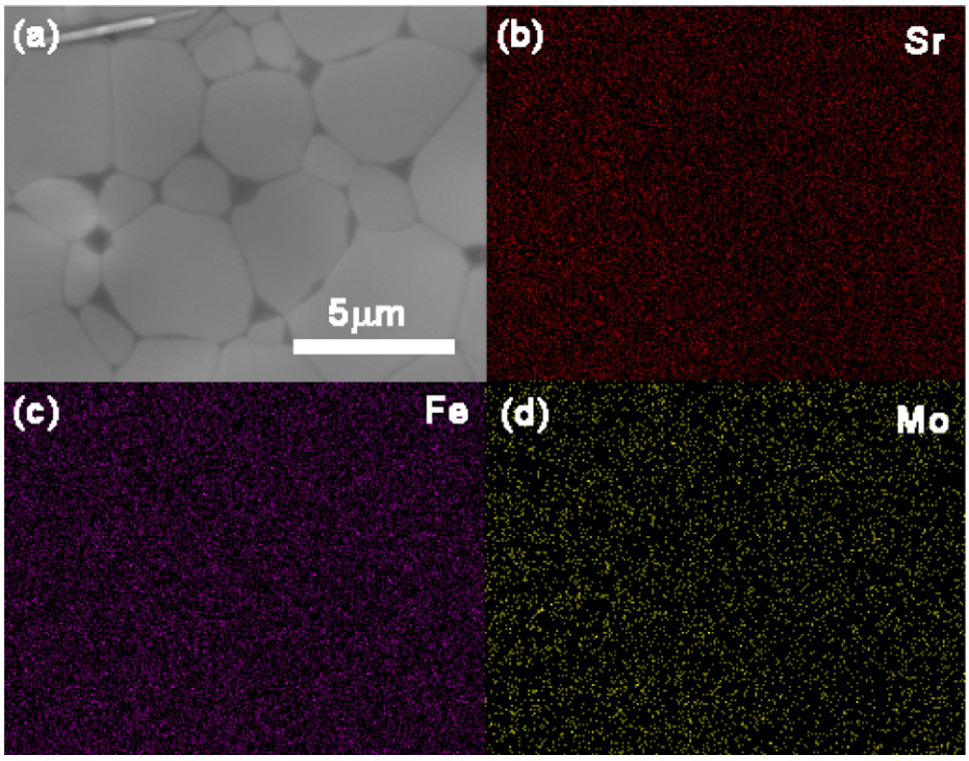

Fig. 4. SEM image (a) and EDX elemental mapping on the fracture surface of the $SrFe_{0.8}Mo_{0.2}O_{3-\delta}$ bar: (b) Sr, (c) Fe and (d) Mo.

where $Fe_{Fe}^{\times}$ and $Fe_{Fe}^{\bullet}$ represent Fe^{3+} and Fe^{4+}, respectively. It can be seen that the electrical conductivity is sensitively affected by the oxygen content and a high oxygen partial pressure is needed for the synthesis of $SrFeO_{3-\delta}$ with high oxygen content. At 300 K, high conductivity ($\sigma \sim 10^3\,S\,cm^{-1}$) has been reported for $Sr_8Fe_8O_{23}$ while the conductivities of $SrFeO_{2.74}$ and $SrFeO_{2.72}$ have been reported to be 10^2 and $10^{-1}\,S\,cm^{-1}$, respectively [23,24]. Considering the synthesis conditions and relatively low conductivity at room temperature of $SrFeO_{3-\delta}$ in our experiment, its oxygen content is probably even lower than 2.72. For Mo-doped $SrFeO_{3-\delta}$, the doping reaction can be expressed as:

$$MoO_3 + \frac{3}{2}V_O^{\bullet\bullet} \overset{SrFeO_{3-\delta}}{\longleftrightarrow} Mo_{Fe}^{\bullet\bullet\bullet} + 3O_O^{\times} \quad (2)$$

where $Mo_{Fe}^{\bullet\bullet\bullet}$ represents Mo^{6+}. Incorporation of Mo will be accompanied by an increase in the oxygen content and decrease in the number of oxygen vacancies. Consequently, Eq. (1) is expected to shift to the left as a compensation for Mo-doping, resulting in a decrease in the number of the charge carrier Fe^{4+}, which may account for the electrical conductivity decrease with Mo-doping. The decrease of Fe^{4+} in Mo-doped $SrFeO_{3-\delta}$ is also revealed from XPS results shown below.

Next, Arrhenius curves of conductivity are plotted in Fig. 5b. Linear relationships can be observed at low temperatures for different samples. According to the small polaron conduction mechanism, if the carrier concentration is constant, the relationship between the conductivity σ and temperature T can be described as [25]:

$$\sigma = \frac{C}{T}\exp\left(\frac{-E_a}{kT}\right) \quad (3)$$

where E_a is the activation energy, k is the Boltzmann constant and C is the pre-exponential constant which includes contributions from the carrier concentration as well as other properties of the material. Therefore, the plots of σT vs. $1000/T$ should be linear. However, the plots shown in Fig. 5b have significant deviations from linearity at higher temperatures. This deviation is probably due to the change in charge carrier concentration at higher temperatures. As reported for other ferrous perovskites, the thermal reduction of Fe^{4+} to lower valence states may be one important reason for this behavior [25]. In Fig. 5b, the transition temperature also increases with Mo-doping, suggesting that the Mo-doped $SrFeO_{3-\delta}$ may have a stronger tolerance to reduction.

The activation energy for the linear part of each plot is also listed in Fig. 5b. The activation energy values range from 0.15 to 0.23 eV and are similar to those reported for electronically conducting perovskite systems, from 0.1 to 0.18 eV for (La, Sr)(Co, Fe)O_3 and from 0.11 to 0.29 eV for (La, Ba)(Co, Fe)O_3 [25]. It can be also noticed that the activation energy decreases with Mo-doping. Similar results were also reported by other groups [18]. Since the conduction of $SrFeO_{3-\delta}$ can be explained by the double exchange mechanism according to which charges transfer through the Fe

Table 1
Fitting results for Fe 2p 3/2 signal.

Mo content x	Peak (I)	Peak (II)	Peak (III)	Average valence state of Fe[a]	Oxygen content[a]
0	47.7%	45.4%	6.9%	3.41	2.70
0.05	37.9%	50.5%	11.6%	3.26	2.70
0.1	37.0%	50.7%	12.3%	3.24	2.76
0.2	34.9%	52.0%	13.1%	3.21	2.89
0.25	30.1%	50.3%	19.6%	3.11	2.91

[a] Assuming that the fitting peaks I–III are attributed to Fe^{4+}, Fe^{3+} and Fe^{2+}, respectively.

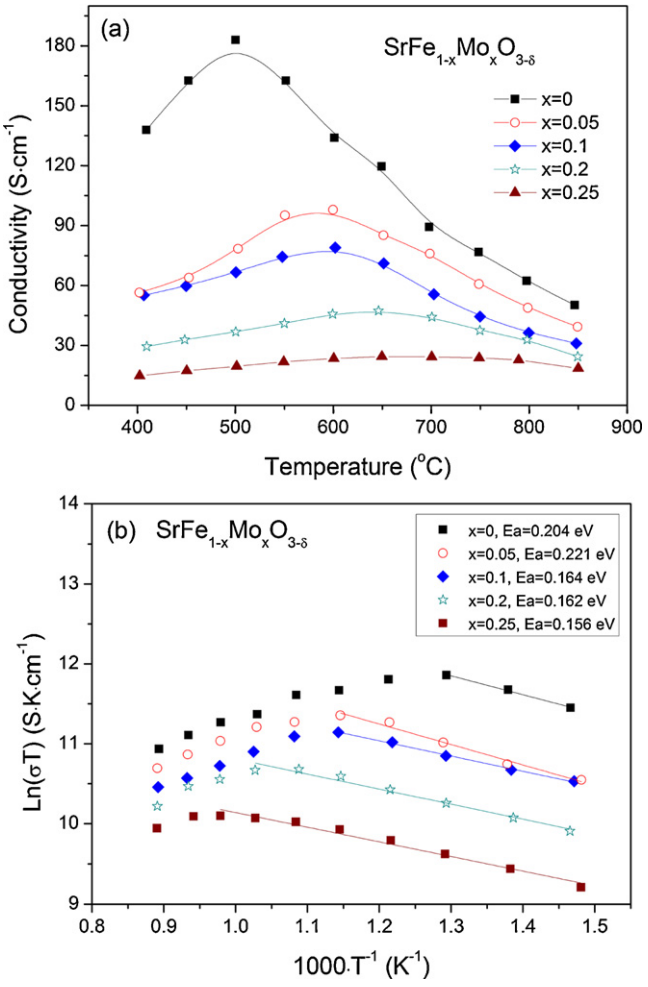

Fig. 5. (a) Electrical conductivities and (b) corresponding Arrhenius plots of the $SrFe_{1-x}Mo_xO_{3-\delta}$ (x = 0, 0.05, 0.1, 0.2 and 0.25) bars in air.

3d–O 2p orbitals, oxygen content affects not only the concentration but also the mobility of holes [8]. Although Mo-doping results in a decrease in conductivity, the suppression of oxygen vacancies by doping with Mo may restore the transport chains for holes and improve their mobility, consequently lowering the activation energy.

The influence of Mo-doping on the valence states of Fe in $SrFe_{1-x}Mo_xO_{3-\delta}$ was investigated by XPS. Fig. 6 shows Fe 2p spectra of different samples. Two peaks of Fe 2p 1/2 and Fe 2p 3/2 can be observed in each spectrum. Considering the synthesis conditions, there may be three valence states of Fe (*i.e.*, +4, +3 and +2) for each sample. In order to compare the spectra of different samples, three peaks with fixed intervals were used to fit the Fe 2p 3/2 signal. The fitting curves are also shown in Fig. 6 and the area ratios of each peak are summarized in Table 1. Clearly, as listed in Table 1, the larger ratio of the fitting peak (I) (with the highest binding energy) reveals the higher valence state of Fe in the sample with the lower Mo content. If it is assumed that the fitting peaks can be attributed to Fe^{4+}, Fe^{3+} and Fe^{2+}, the average valence state of Fe as well as the oxygen content in different samples can also be estimated. As listed in Table 1, Mo-doping increased the oxygen content and lowered the Fe^{4+} concentration in the samples. These results are consistent with those obtained by XRD and conductivity measurements in this work, as well as those reported previously in the literature [26].

The TPR profile, the TG, and differential thermogravimetry (DTG) curves of $SrFeO_{3-\delta}$ are compared in Fig. 7. There are three major peaks in the TPR profile located approximately at 450 and 580 and

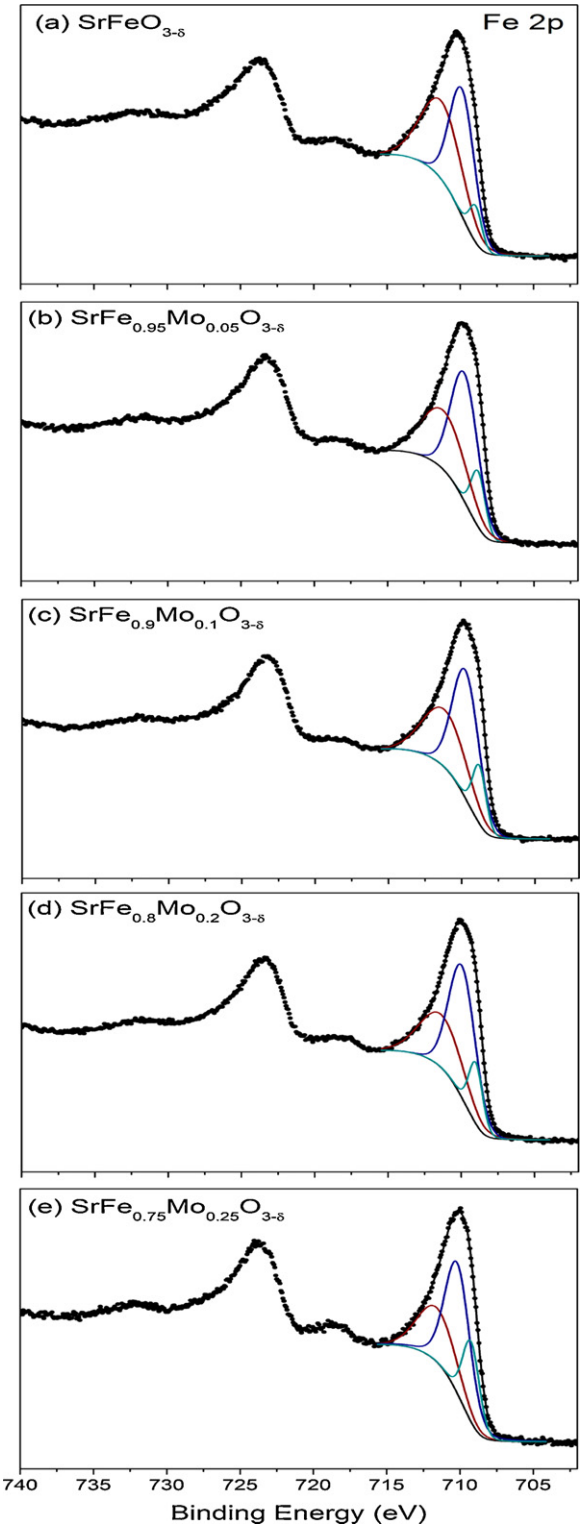

Figure 6. Fe 2p core-level spectra (points) and the fitting results (lines) for $SrFe_{1-x}Mo_xO_{3-\delta}$ (a) x = 0, (b) x = 0.05, (c) x = 0.1, (d) x = 0.2, and (e) x = 0.25.

870 °C, respectively. According to the literature, $SrFeO_{3-\delta}$ can be fully reduced to $SrFeO_{2.5}$ at 500 °C following an overnight treatment in a 5% H_2/N_2 mixture, indicating that reduction of Fe^{4+} to Fe^{3+} may be responsible for the shoulder peak at approximately 450 °C [6]. The other two TPR peaks may be attributed to the reduction of Fe^{3+} to Fe^{2+} and Fe^{2+} to Fe^0, respectively. In Fig. 7b, the TG curve shows continuous weight loss when increasing the temperature and peaks

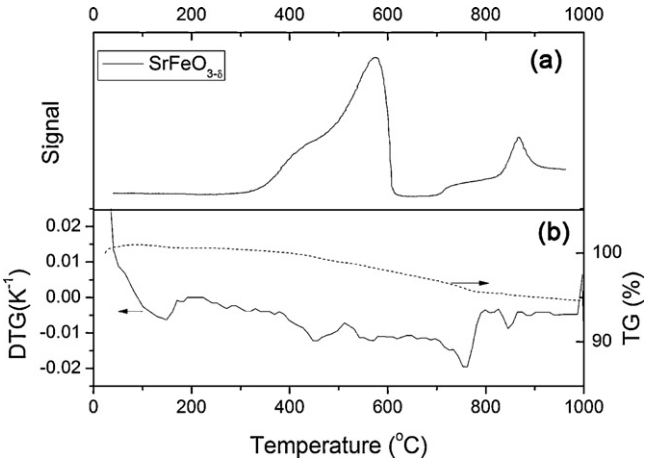

Fig. 7. (a) TPR, (b) *ex situ* DTG and TG spectra of $SrFeO_{3-\delta}$ in a 5% H_2/N_2 mixture.

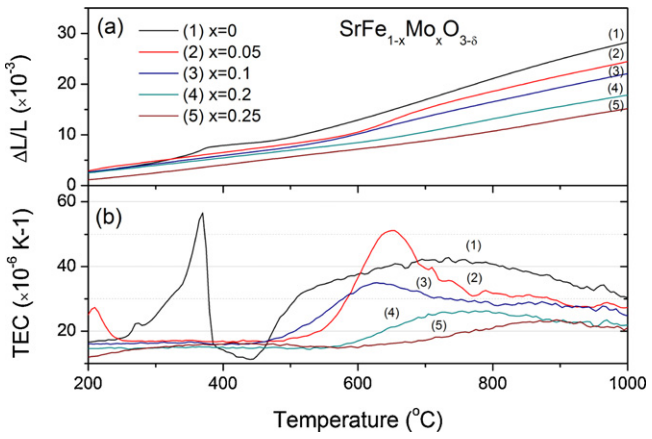

Fig. 9. (a) Thermal expansion and (b) thermal expansion coefficient measured from room temperature to 1000 °C in air for $SrFe_{1-x}Mo_xO_{3-\delta}$ (x = 0, 0.05, 0.1, 0.2 and 0.25).

in the DTG curve indicate rates of mass change at certain temperatures. Since the sample was not degassed prior to the TG test, weight loss below 200 °C may be related to desorption of moisture and other absorbed species. However, all the reduction processes shown in the TPR profile can be tracked by the corresponding mass loss in the DTG curve in Fig. 7b.

Fig. 8 shows the TPR profiles of the Mo-doped samples. Similar reduction peaks were observed in all cases. However, the position of these peaks has shifted to lower temperatures. This shift is probably due to the interaction between Fe and Mo cations. It is also evident that the shoulder peak is weakened when the Mo content is increased, suggesting that the concentration of Fe^{4+} is lower in the sample with the higher Mo content, in agreement with the results discussed above. Additionally, the total area of the reduction peaks decreases and the peak located above 800 °C – assigned to the reduction of Fe^{2+} to Fe^0 – becomes smaller when the Mo doping ratio increases. These results also indicate that the tolerance to reduction of the material is improved by doping with Mo.

Thermal expansion behavior of different samples was investigated in air and the results are shown in Fig. 9. Obviously, the thermal expansion becomes smaller with more Mo doping. TECs at different temperatures are determined by differentiation of the spectra shown in Fig. 9a. As shown in Fig. 9b, all samples exhibit similar TECs when the temperature is below 450 °C, except for $SrFeO_{3-\delta}$. A large variation of the TEC can be observed for $SrFeO_{3-\delta}$ at approximately 350 °C, which is probably due to the phase transition. Due to the thermal reduction, the TECs of different samples start to increase when the temperature is raised above 500 °C. It is interesting to notice that the starting temperatures for this increase are also different for the different samples. Similarly to the conduction behavior, the sample with the higher Mo content shows the higher transition temperature and lower TEC. At 800 °C in air, the TEC for $SrFe_{0.8}Mo_{0.2}O_{3-\delta}$ is approximately $25.7 \times 10^{-6}\,K^{-1}$. It becomes even lower to $20.9 \times 10^{-6}\,K^{-1}$ for $SrFe_{0.75}Mo_{0.25}O_{3-\delta}$, which has been previously reported as a redox stable cathode material [21]. Similar to cobalt-based cathode materials, the TECs of $SrFe_{0.75}Mo_{0.25}O_{3-\delta}$ are still much higher than those of electrolyte materials at 800 °C.

Cathode performance of these materials is investigated by comparing their polarization resistance in a symmetrical half-cell configuration. However, due to the low sintering ability and the large TEC of $SrFeO_{3-\delta}$ and $SrFe_{0.95}Mo_{0.05}O_{3-\delta}$, the electrodes were easily peeled off in these cases from the electrolyte after the current collector was applied. As shown in Fig. 10, results were only obtained with $SrFe_{0.9}Mo_{0.1}O_{3-\delta}$ and $SrFe_{0.8}Mo_{0.2}O_{3-\delta}$. The ohmic and polarization resistance are still very large for $SrFe_{0.9}Mo_{0.1}O_{3-\delta}$ due to the poor connectivity between the electrode and the electrolyte. However, at 800 °C in air, the polarization resistance is only 0.074 Ω cm² for $SrFe_{0.8}Mo_{0.2}O_{3-\delta}$. This value is even lower than that

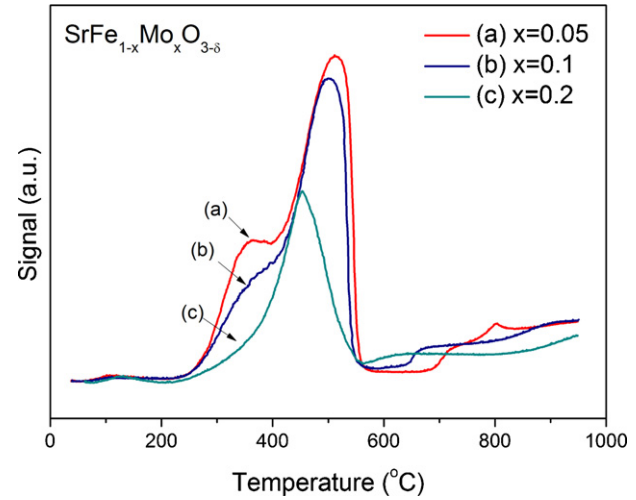

Fig. 8. TPR profiles of $SrFe_{1-x}Mo_xO_{3-\delta}$ (a) x = 0.05, (b) x = 0.1 and (c) x = 0.2 in a 5% H_2/N_2 mixture.

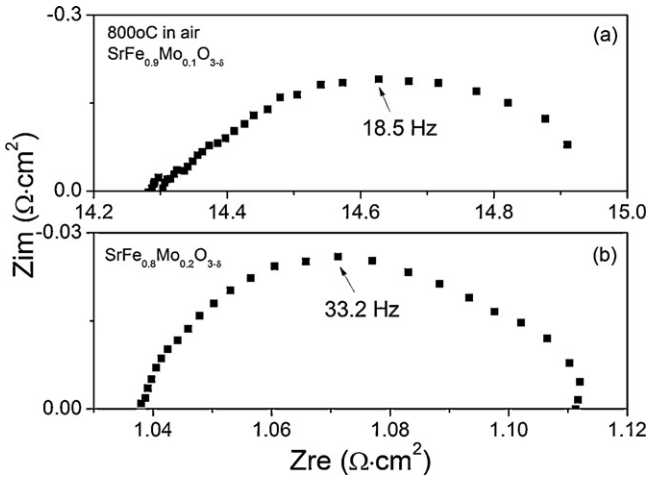

Fig. 10. Polarization resistance of (a) $SrFe_{0.9}Mo_{0.1}O_{3-\delta}$ and (b) $SrFe_{0.8}Mo_{0.2}O_{3-\delta}$ measured in air at 800 °C.

of $SrFe_{0.75}Mo_{0.25}O_{3-\delta}$ ($0.110\,\Omega\,cm^2$) under similar testing conditions [21]. These results can be attributed to the decrease in both the electronic and ionic conductivity of $SrFeO_{3-\delta}$ by Mo-doping, which in turn may result in different polarizations of oxygen reduction on the materials examined [18,19].

4. Conclusion

By doping with a certain amount of Mo, doped $SrFe_{1-x}Mo_xO_{3-\delta}$ perovskites can be stabilized in a cubic structure in air and their sintering ability can be improved. The electrical conductivity in air is reduced with increasing Mo content. When the doping ratio was increased to 0.25, the conductivity dropped to about $22\,S\,cm^{-1}$ at 800 °C. This decrease is probably due to a decrease of charge carriers, as indicated by the XPS and TPR results. The TPR profiles further revealed that the tolerance of $SrFeO_{3-\delta}$ to reduction was also improved by Mo-doping. $SrFeO_{3-\delta}$ exhibited a large thermal expansion coefficient in air when the temperature was above 500 °C (about $40 \times 10^{-6}\,K^{-1}$ at 800 °C). By doping with Mo, this value was decreased to $25.7 \times 10^{-6}\,K^{-1}$ for $SrFe_{0.8}Mo_{0.2}O_{3-\delta}$ and $20.9 \times 10^{-6}\,K^{-1}$ for $SrFe_{0.75}Mo_{0.25}O_{3-\delta}$ at 800 °C. Considering the acceptable conductivity, high tolerance to reduction and relatively low polarization resistance, the Mo-doped $SrFeO_{3-\delta}$ perovskite can be applied as potential cathode materials for SOFCs.

Acknowledgement

This paper is based on work supported as part of the HeteroFoaM Center (Heterogeneous Functional Materials for Energy Systems), an Energy Frontier Research Center (EFRC) funded by the Department of Energy Office of Science, Office of Basic Energy Sciences under Award Number DE-SC0001061.

References

[1] B.C.H. Steel, Nature 400 (1999) 619–621.
[2] S.C. Singhal, Solid State Ionics 135 (2000) 305–313.
[3] J. Yoo, A. Verma, S. Wang, A.J. Jacobson, J. Electrochem. Soc. 152 (2005) A497–A505.
[4] V. Zaspalis, A. Evdou, L. Nalbandian, Fuel 89 (2010) 1265–1273.
[5] Y. Niu, W. Zhou, J. Sunarso, L. Ge, Z. Zhu, Z. Shao, J. Mater. Chem. 20 (2010) 9619–9622.
[6] J.P. Hodges, S. Short, J.D. Jorgensen, X. Xiong, B. Dabrowski, S.M. Mini, C.W. Kimball, J. Solid State Chem. 151 (2000) 190–209.
[7] V. Vashuk, L. Kokhanovskii, I. Yushkevich, Inorg. Mater. 36 (2000) 79–83.
[8] M.V. Patrakeev, I.A. Leonidov, V.L. Kozhevnikov, V.V. Kharton, Solid State Sci. 6 (2004) 907–913.
[9] Y. Tsujimoto, C. Tassel, N. Hayashi, T. Watanabe, H. Kageyama, K. Yoshimura, M. Takano, M. Ceretti, C. Ritter, W. Paulus, Nature 450 (2007) 1062–1065.
[10] P. Adler, A. Lebon, V. Damljanovicacute, C. Ulrich, C. Bernhard, A.V. Boris, A. Maljuk, C.T. Lin, B. Keimer, Phys. Rev. B 73 (2006) 094451.
[11] M. Schmidt, S.J. Campbell, J. Solid State Chem. 156 (2001) 292–304.
[12] Y. Niu, J. Sunarso, F. Liang, W. Zhou, Z. Zhu, Z. Shao, J. Electrochem. Soc. 158 (2011) B132–B138.
[13] S.P. Simner, J.F. Bonnett, N.L. Canfield, K.D. Meinhardt, V.L. Sprenkle, J.W. Stevenson, Electrochem. Solid-State Lett. 5 (2002) A173–A175.
[14] J. Mizusaki, M. Okayasu, S. Yamauchi, K. Fueki, J. Solid State Chem. 99 (1992) 166–172.
[15] G. Liu, G. Rao, X. Feng, H. Yang, Z. Ouyang, W. Liu, J. Liang, J. Alloys Compd. 353 (2003) 42–47.
[16] L. Zhang, Q. Zhou, Q. He, T. He, J. Power Sources 195 (2010) 6356–6366.
[17] G. Xiao, Q. Liu, X. Dong, K. Huang, F. Chen, J. Power Sources 195 (2010) 8071–8074.
[18] A.A. Markov, I.A. Leonidov, M.V. Patrakeev, V.L. Kozhevnikov, O.A. Savinskaya, U.V. Ancharova, A.P. Nemudry, Solid State Ionics 179 (2008) 1050–1053.
[19] O. Savinskaya, A. Nemudry, J. Solid State Electron. 15 (2011) 269–275.
[20] Q. Liu, X. Dong, G. Xiao, F. Zhao, F. Chen, Adv. Mater. 22 (2010) 5478–5482.
[21] G. Xiao, Q. Liu, F. Zhao, L. Zhang, C. Xia, F. Chen, J. Electrochem. Soc. 158 (2011) B455–B460.
[22] H. Falcón, J.A. Barbero, J.A. Alonso, M.J. Martínez-Lope, J.L.G. Fierro, Chem. Mater. 14 (2002) 2325–2333.
[23] J. Hombo, Y. Matsumoto, T. Kawano, J. Solid State Chem. 84 (1990) 138–143.
[24] S. Nakamura, S. Iida, Jpn. J. Appl. Phys. 34 (1995) L291–L293.
[25] J.W. Stevenson, T.R. Armstrong, R.D. Carneim, L.R. Pederson, W.J. Weber, J. Electrochem. Soc. 143 (1996) 2722–2729.
[26] Z. Šimša, J. Šimšová, P.E. Zemek, M. Wigen, Pardavi-Horvath, J. Phys. Colloques 49 (1988), pp. C8-975–C8-976.